[4] K. Tomiyasu, "Tutorial review of synthetic-aperture radar (SAR) with applications to imaging of the ocean surface," *Proc. IEEE*, vol. 66, pp. 563–583, May 1978.
[5] J. C. Curlander and R. N. McDonough, *Synthetic Aperture Radar. Systems and Signal Processing*. New York: Wiley, 1991.
[6] R. O. Harger, *Synthetic Aperture Radar Systems—Theory and Design*. New York: Academic, 1970, p. 29.
[7] F. K. Li *et al.*, "Ambiguities in spaceborne synthetic aperture radar systems," *IEEE Trans. Aerospace Electron. Syst.*, vol. AES-19, pp. 389–395, May 1983.
[8] K. Tomiyasu, "A note on specular ocean surface radar cross section," *J. Geophys. Res.*, vol. 79, p. 3101, July 20, 1974.

Radar Estimates of Aboveground Biomass in Boreal Forests of Interior Alaska

Eric Rignot, JoBea Way, Cynthia Williams, and Leslie Viereck

***Abstract*—Airborne SAR data gathered by the NASA/JPL three-frequency, polarimetric, radar system in winter, spring, and summer over the Bonanza Creek Experimental Forest, near Fairbanks, AK, are compared to estimates of whole-tree aboveground dry biomass from 21 forest stands and two clear-cuts. While C-band radar backscatter shows little sensitivity to biomass, L- and P-band radar backscatter increase by more than 6 dB when biomass increases from 5 to 200 tons/ha. Using second-order polynomial regressions, biomass values are predicted from the radar at L- and P-band and compared to actual biomass values. At P-band HV-polarization, the error in predicted biomass is about 30% of the actual biomass. When HV-, HH-, and VV-polarization are used together in the regression, the error in predicted biomass is about 20%. Errors obtained using L-band data are a few percents larger. These errors are caused by uncertainties in actual stand biomass estimates, significant inner-stand spatial variations in biomass, unusual conditions of forest stands following natural disturbances, along with interactions of the radar signals with a complex three-dimensional structure of the canopy. Multiple incidence angle data reveal that the incidence angle θ_i of the radar illumination is also a factor influencing the retrieval of biomass, even at HV-polarization, when $\theta_i > 50°$ or $\theta_i < 25°$. Finally, the radar response of the forest—and thereby the regression curves for biomas retrieval—are dependent on the seasonal and environmental conditions.**

I. Introduction

Recent experiments using airborne active microwave data indicate forest biomass could be quantified remotely [1]–[3]. Radar backscatter was shown to be positively correlated with total aboveground dry biomass until it saturates at a level which is higher with increasing radar wavelengths. The results provide evidence that inversion algorithms could be developed for predicting forest biomass from long wavelength SAR data. At the same time, these studies have been limited to the examination of undisturbed, even-aged, monospecie plantations of pine trees in temperate regions, with nearly level topography. Modeling and simulation results [4]–[7] suggest that the effect on radar backscatter of tree structure, vegetation moisture condition and status, as well as understory condition and topography can be significant and thereby complicate the inference of aboveground biomass from the radar. Before operational applications are developed it is necessary to investigate experimentally the relative magnitude of these effects in natural forest ecosystems.

Here we examine the relationship between radar backscatter and aboveground biomass in a natural forest setting, with mixtures of coniferous and deciduous tree species, strongly varying environmental conditions, and level to moderate topography. The forest site is the Bonanza Creek Experimental Forest (BCEF), a Long Term Ecological Research (LTER) site located at 64° 45'N, −148°W, in the proximity of Fairbanks, AK, along the Tanana river. SAR data were gathered at BCEF on several occasions and at different seasons by the three-frequency NASA/JPL polarimetric airborne radar system (AIRSAR). BCEF is in the midst of the boreal forested biome which is believed to play an important role in the global carbon cycle [8]–[12]. Boreal forests are a major reservoir of live carbon, only second to broadleaf humid forests, and are thought to be responsible for the seasonal variations in atmospheric CO_2 observed at the northern latitudes. Mapping and monitoring of whole-tree aboveground biomass in these forests is therefore particularly relevant to studies of the global carbon cycle.

II. Methods

A. Study Area

The vegetation landscape at BCEF is a mosaic of forest, grassland, shrubs, bog, and tundra types that have formed primarily as a result of slope, aspect, elevation, parent material, and succession after wildfire [13]–[15] (Fig. 1). Presence or absence of permafrost, and solar illumination angle, both correlated with slope and aspect, are dominant factors in the distribution of vegetation types. The forest site includes both upland fire-controlled succession, and floodplain succession forests. Upland forest types vary from highly productive aspen (*Populus tremuloides*), paper birch (*Betula papyrifera*), and white spruce (*Picea glauca*) stands on well-drained, nutrient-rich, warm, permafrost-free, south-facing slopes, to black spruce (*Picea mariana*) forests on poorly drained, nutrient-poor, permafrost soils of north-facing slopes, lowlands, and lower slopes. In mature white spruce stands in the uplands, dominant tree sizes average about 30 cm DBH (diameter at breast height) and 25–35 m in height, with tree densities about 500–1000 stems/ha. Standing aboveground tree biomass ranges from 92 to 183 tons/ha for the hardwood stands up to 249 tons/ha for white spruce stands. In mature, black spruce, upland stands, dominant tree sizes average about 6–15 cm, and 5–10 m in height, with tree densities about 1400–4000 stems/ha. Aboveground biomass ranges from 2 to 11 tons/ha.

Floodplain forests vary from productive stands of balsam poplar (*Populus balsamifera*) and white spruce forming on river alluvium, permafrost-free soils, to slow-growing black spruce and bogs occupying older terraces underlained by permafrost. Young successional stages are dominated by alder (*Alnus tenuifolia*) and willow shrubs (*Salix spp.*), followed by extensive stands of balsam poplar and the mature stages of well-developed stands of white spruce. In mature, white spruce stands, dominant tree sizes average about 30 cm DBH and 25–35 m in height, and tree densities are high (1000 stems/ha). Aboveground tree biomass ranges from 40–180 tons/ha for balsam poplar stands to 60–245 tons/ha for white spruce stands. Black spruce is the most widespread forest type, covering 44% of

Manuscript received December 20, 1993; revised May 9, 1994. This work was carried out at the Jet Propulsion Laboratory, California Institute of Technology, under contract with the National Aeronautics and Space Administration.

E. Rignot and J. Way are with the Jet Propulsion Laboratory, California Institute of Technology, Pasadena CA 91109.
C. Williams and La Viereck are with the Institute of Northern Forestry, U.S. Forest Service, Fairbanks, AK 99775.

IEEE Log Number 9403642.

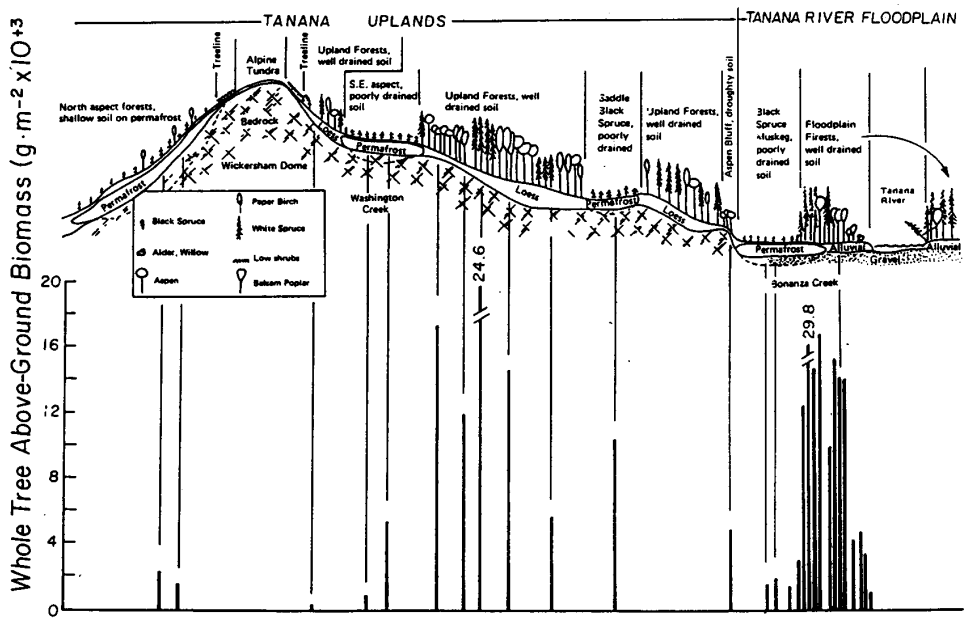

Fig. 1. Composite cross-section showing the distribution of forest vegetation types with topography in the Tanana uplands and lowlands in the Fairbanks vicinity. Whole-tree above-ground dry biomass is presented for selected vegetation types [7].

the area and usually associated with permafrost. Low-land mature black spruce forests are similar to upland black spruce forests.

The climate at BCEF is continental, with large diurnal temperature variations, low precipitation, low cloud cover and low humidity [16]. Mean annual temperature is −3.5°C, and temperature extremes range from +35°C in June to −65°C in January. The annual mean precipitation is 286 mm, with 30% falling as snow.

B. Airborne SAR Data

AIRSAR is a polarimetric radar imager operating at P- (68 cm wavelength), L- (24 cm) and C-band (5.6 cm) frequencies simultaneously [17]. AIRSAR imaged BCEF on March 13, 17, and 19 of 1988 when the forest changed from frozen (March 11) to thawed conditions (March 13) and back to frozen conditions (March 17) due to a transition to unusually ware air-temperatures for the season [18]. On May 4, 6, and 7 of 1991, AIRSAR overflew the study site when the forest changed from flooded (May 4) to unflooded conditions (May 6–7) with the formation and subsequent disappearance of ice jams in the Tanana river. Finally, AIRSAR overflew BCEF in the Summer of 1993, with clear skies and dry climatic conditions. Data calibration was performed in a similar fashion for all data takes using the calibration procedure described in [19] and 1.8 m trihedral corner reflectors deployed on the ground in clear-cut areas prior to each of the SAR overflights. The SAR data were subsequently projected onto ground-range, resampled to a common pixel spacing, and co-registered to the scene acquired on May 6, 1991 using the registration procedure for polarimetric SAR data described in [20]. All data takes considered in this study were acquired at a look angle of 40° unless mentioned otherwise.

C. Ground Data Collection

Between 1988 and 1993, 21 forest stands were inventoried for tree density, DBH, height, canopy depth, and species. Aerial photographs were used to determine the starting point and transect direction for each stand. The first plot was started well enough within the stand to avoid any edge effects from the river, adjacent clear-cuts, and other stands. Ten plots were sampled in each stand, separated by about 100 m, eventually reduced to 50 m in smaller stands. Transects turned in many instances to stay within stand boundaries and to avoid anomalies such as old river sloughs. Plot radii were chosen to include roughly 15 live trees (a "live" tree has a DBH > 2.5 cm) providing a sampling of 150 trees per stand. While all DBH's were measured, not all trees were measured for tree height. In each stand, only 40 trees of each species present in the overstory were chosen for height measurements. From the DBH and height data collected in the field, linear regressions relating DBH and height of measured trees were derived and then used to estimate heights of the trees for which height had not been measured. Whole-tree aboveground biomass was then estimated for each tree using empirical, allometric equations from Manning *et al.* [21], Singh [22], and Yarie and Van Cleve [23] for all tree species except alder for which we used a linear regression analysis developed by the Forest Soils Laboratory, University of Alaska, Fairbanks. Biomass values for each tree were subsequently averaged over each plot, and biomass values for the plots were used to compute the average and standard deviation of the stand biomass. The inventory results are summarized in Table I.

The transect boundaries of each stand were drawn on the computer to within a few SAR pixels (about 30 m) of their actual position recorded on aerial photos. Calibrated radar backscatter values, σ°, were then extracted from each stand at each frequency and polarization and averaged together over the whole stand. Even for the smallest stands, several hundred independent SAR samples were averaged together so σ° is not affected by image speckle. To compute the standard deviation in σ°, we used the statistical model described in [24] to remove the contribution from speckle (1991 and 1993 AIRSAR data are 16-looks; 1988 AIRSAR data are

TABLE I

STATIC CHARACTERISTICS OF 21 FOREST STANDS FROM BCEF, ALASKA. WS IS WHITE SPRUCE, BP IS BALSAM POPLAR, BS IS BLACK SPRUCE, BP IS BALSAM POPLAR. AL IS ALDER, BIR IS BIRCH, TA IS TAMARACK, AND WI IS WILLOW. TREE SPECIES COMPOSITION ARE SHOWN IN % BASED ON THE NUMBER OF TREES PER SPECIES PER STAND. WS40, WS41, WS42, AND PBW40 ARE FROM THE UPLANDS. ALL OTHER STANDS ARE FROM THE FLOODPLAINS. IN THE FIRST COLUMN, (yr) INDICATES THE YEAR THE STAND WAS SAMPLED. ANGLE IS THE LOCAL INCIDENCE ANGLE OF THE RADAR ILLUMINATION COMPUTED AT THE CENTER OF THE FOREST STAND FOR THE SCENE ACQUIRED ON MAY 6, 1991, BASED ON BOTH IMAGING GEOMETRY AND LOCAL TOPOGRAPHY PROVIDED BY A DIGITAL ELEVATION MODEL FROM THE U.S. GEOLOGICAL SURVEY

STAND (yr)	Stems #/ha	Height m	Age yr	DBH cm	Sum. B. tons/ha	Win. B. tons/ha	Tree Species %	Angle (deg)
WS1 (88)	1246	22.1	165	19.6	217 (88)	217 (88)	WS 91 : BIR 8 : BP 1	35.3
WS2 (88)	2073	20.1	100	14.5	167 (36)	167 (36)	WS 91 : BP 7 : AL 2	35.6
WS3 (92)	860	18.8	125	19.8	172 (38)	173 (38)	WS 89 : BIR 6 : BS 3 : BP 2	35.6
WS4 (90)	608	22.0	124	25.0	164 (55)	163 (55)	WS 85 : BIR 15	36.7
WS5 (88)	1484	21.3	180	17.9	181 (48)	181 (48)	WS 97 : BP 3	35.6
WS7 (88)	1123	24.5	120	21.4	215 (61)	215 (61)	WS 97 : BP 2 : BIR 1	42.4
WS23 (90)	1135	12.3	200	13.9	61 (13)	61 (13)	WS 71 : BS 12	33.2
WS40 (92)	573	19.4	118	21.8	196 (41)	196 (41)	WS 89 : BIR 10 : BP 1	39.9
WS41 (93)	278	20.0	153	23.4	218 (60)	218 (60)	WS 88 : BP 9 : BIR 3	40.6
WS42 (93)	353	20.0	134	24.0	109 (46)	109 (46)	WS 96 : BIR 4	50.1
WSBP1 (90)	4997	10.4	50	9.3	110 (32)	109 (32)	WS 89 : BP 11	42.4
WSBP2 (92)	1060	14.5	75	15.4	137 (62)	136 (62)	WS 82 : BP 18	40.6
BS1 (88)	1975	7.6	200	8.8	37 (8)	37 (8)	BS 90 : TA 7 : WS 2 : BIR 1	38.5
BS2 (90)	1402	6.8	200	8.2	23 (5)	23 (5)	BS 95 : TA 5	41.6
BS4 (92)	1487	4.3	67	4.4	6 (4)	6 (4)	BS 60 : TA 40	51.2
BP2 (88)	1615	18.9	90	17.0	182 (109)	179 (107)	BP 92 : WS 6 : AL 2	33.9
BP13 (90)	1125	15.2	75	18.5	106 (29)	104 (28)	BP 53 : WS 47	38.8
BP14 (91)	1538	12.6	NA	13.3	85 (67)	85 (69)	BP 90 : WS 10	41.6
BP6 (90)	3699	9.1	30	7.3	36 (7)	34 (7)	BP 43 : AL 53	44.1
AL1 (90)	7904	6.9	30	5.0	29 (10)	27 (10)	AL 79 : WI 21	38.8
PBW40 (93)	471	19.4	NA	23.7	105 (41)	103 (40)	BIR 81 : WS 19	52.4

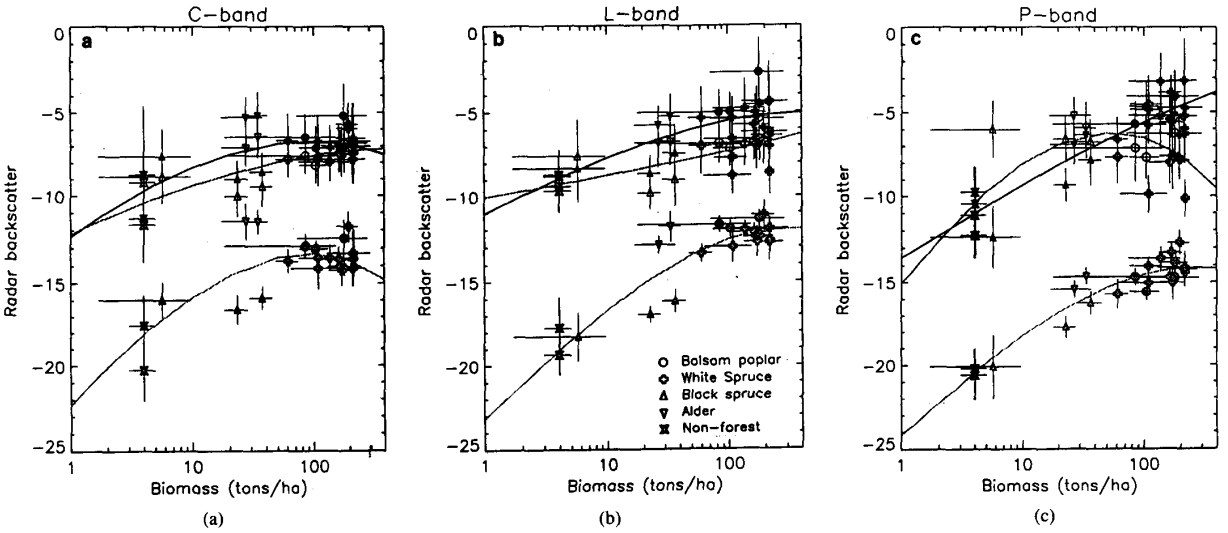

Fig. 2. Radar backscatter σ° (in decibels) at HH- (black dots), HV-(gray dots), and VV-(white dots) polarization (H means horizontal and V means vertical) of 21 forest stands versus whole-tree aboveground dry biomass (in tons/ha) in log-log scale at (a) C-band; (b) L-band; (c) P-band on May 6, 1991. Thin horizontal and vertical bars correspond, respectively, to the standard deviations in biomass and σ° for each forest stand. Continuous lines are third-order polynomial regressions relating σ° in dB to the logarithm of the stand biomass. The biomass level of clear-cuts was estimated from the results in [14].

4-looks) and obtain a measure of the natural spatial variability in σ° or "texture" of the forest.

III. RESULTS

The calibrated radar response σ° of the forest on May 6, 1991 is shown in Fig. 2 as a function of whole-tree aboveground dry biomass. The data acquired in winter and summer are discussed later on in the paper. As σ° eventually approaches a saturation level at the high biomass levels, third-order polynomials were fit to the data instead of straight lines (Fig. 2). The results show that σ° is positively correlated with aboveground biomass. In contrast, the normalized difference vegetation index (NDVI) of the same forest stands computed from a SPOT scene acquired on August 8, 1991 [25] is not correlated with biomass (Fig. 3). Although NDVI could be used to distinguish deciduous species (alder and balsam poplar with higher NDVI) from coniferous species (black spruce and white spruce with lower NDVI), NDVI does not provide indications on the relative biomass level of each forest stand.

At C-band [Fig. 2(a)], σ°_{HV} increases with biomass until it satu-

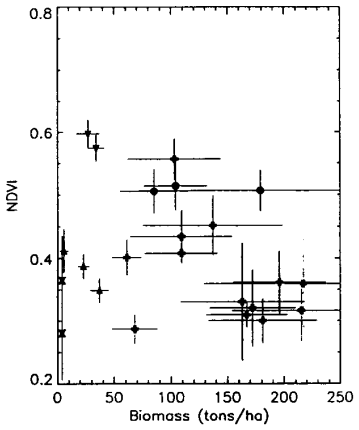

Fig. 3. Normalized Difference Vegetation Index (NDVI) values extracted from a SPOT scene acquired on August 28, 1991 over BCEF, versus whole-tree aboveground biomass. DN values were converted to radiances [25].

rates at a biomass level less than 50 tons/ha; and σ°_{HH} and σ°_{VV} are not sensitive to forest biomass. This trend is consistent with past observations of other forest types as well as modeling studies [1]–[7]. C-band radar signals moderately penetrate the forest canopy and are mainly scattered by the foliage and branches and twigs of the upper canopy. Hence, σ° quickly saturates as biomass increases. At the same time, C-band signals are very sensitive to differences in canopy structure (size, orientation, and density of branches, twigs, leaves or needles) and separate different tree species well, especially at HV-polarization [25].

At L-band, σ° is positively correlated with forest biomass [Fig. 2(b)]. L-band signals are expected to penetrate deeper inside the tree canopy than C-band signals and to be scattered mostly by larger branches and the trunk (the biomass of which is correlated to total biomass). The dynamic range in σ°_{HV} between 5 and 200 tons/ha is 4 dB grater than that measured at C-band, and σ°_{HV} saturates at about 100 tons/ ha. σ°_{HH} and σ°_{VV} offer less sensitivity to biomass than σ°_{HV}.

At P-band, the dynamic range in σ°_{HV} between 5 and 200 tons/ha is about the same as that measured at L-band [Fig. 2(c)]. The most striking difference with L-band data is the much higher sensitivity of H-polarization to biomass. The dynamic range in σ°_{HH} is as large as that observed for σ°_{HV}, and the difference between σ°_{HH} and σ°_{VV} increases with increasing biomass. One possible explanation is that radar signals interact more strongly with the tree-trunks at P-band than at L-band. These interactions are likely dominated by double bounce scattering from the tree-trunks to the forest floor back to the radar direction. Modeling studies showed that double bounce scattering increases with tree height and therefore should become significant compared to volume scattering from the branches at the high biomass levels; double bounce scattering is more effective at the longer wavelengths because the signals are less attenuated during propagation through the canopy and are scattered by larger objects, and therefore should be stronger at P-band than at L-band; and double bounce scattering is stronger at HH-polarization than at VV-polarization because V-polarized signals are more attenuated during propagation through the tree-trunks. Hence, a more effective contribution of backscattering from the trunks compared to backscattering from the branches could explain the enhanced sensitivity of σ°_{HH} to biomass at P-band, as well as $\sigma^\circ_{VV} < \sigma^\circ_{HH}$ at the high biomass levels. Another important feature of the P-band radar response from the forest is that data dispersion associated with difference in forest type is reduced compared to that observed at the other two frequencies (Fig. 2). For instance, data points for alder and black spruce stands are on the same regression curve on Fig. 2c while they were not in Fig. 2(a), (b). Hence, it may be easier to use a single inversion curve for all tree species at P-band than at L- or C-band.

IV. Radar Estimates of Aboveground Biomass

Using the data shown in Fig. 2, we derived regression curves relating the logarithm of biomass to second-order polynomials in the logarithm of σ°_{HV}, σ°_{HH}, or σ°_{VV} at one frequency, i.e., of the form: Log $B = \Sigma_{i=0}^{i=2} a_i \sigma^{\circ i}_{XY}$ where B is the stand biomass, $\sigma^{\circ i}_{XY}$ is expressed in decibels, X's and Y's are H's or V's, and a_i's are the coefficients of the polynomial. Biomass is then predicted from the radar measurements and compared to inventory estimates (Fig. 4). As a first step, the effect of the incidence angle, θ_i, is ignored in the analysis. All stands were imaged with $35^\circ < \theta_i < 45^\circ$ for which σ° is expected to vary by less than ± 1 dB. The error of the inversion is measured as the average absolute difference between predicted biomass and actual biomass divided by actual biomass and multiplied by 100, and is expressed in percent (Table II).

At L-band HV, the radar largely overestimates the biomass of alder stands. When alder stands are included, the error rate is 75%, whereas when alder stands are ignored it is 39%. One reason is that σ°_{HV} of alder trees at L-band is higher than expected from their relatively low biomass level, and we use the same inversion curve for all tree species. For clear-cuts, black spruce, and young stands of white spruce the radar estimates are accurate below a 100 tons/ha. Above that level, data dispersion increases. The results improve slightly when σ°_{HH} and σ°_{VV} are also used in the regression as the error rate drops by 4% (Table II).

Radar predictions at P-band HV are more accurate than at L-band HV and extend over almost the entire range of biomass level for these forests [Fig. 4(c)]. The error rate without alder trees is 29% (Table II), and 54% when including alder trees. Adding σ°_{HH} and σ°_{VV} to the regression significantly improves the results. The error rate drops to 21% without alder trees and 33% otherwise. The biomass level of alder trees is more correctly estimated. One reason is that $\sigma^\circ_{HH} \ll \sigma^\circ_{VV}$ for alder trees whereas at the high biomass levels $\sigma^\circ_{HH} \gg \sigma^\circ_{VV}$. Indeed, it is expected that trunk-ground interactions would be low in magnitude in alder stands compared to volume scattering from the branches because alder trees are typically short (Table I). One exception is BP6 for which the predicted biomass is too high. Yet, BP6 is not a pure stand of alder as it contains a large proportion of tall balsam poplar trees which can yield strong trunk-ground interactions. BP6 was also flooded on May 4 and probably still wet on May 6, which increases the likelihood of observing higher than usual trunk-ground interactions in that stand. Similarly, large errors are found in other stands exhibiting particular conditions. For instance, BP14 is a very heterogeneous stand with a large uncertainty in actual biomass (Table I) and the radar does not accurately predict biomass in that stand. The radar also overpredicts forest biomass in WSBP2, a stand known for exhibiting enhanced radar backscatter in all radar data takes compared to other stands of balsam poplar. We recently found out that most balsam poplar trees within the stand are rotten, with very high dielectric constant values for the tree trunks. A higher than usual water content for those trees may be the reason for the enhanced radar backscatter from the tree-trunk observed in WSBP2 and an overestimation of biomass.

A similar inversion was performed using the radar data acquired on July 21, 1993. However, only 19 stands could be used in the

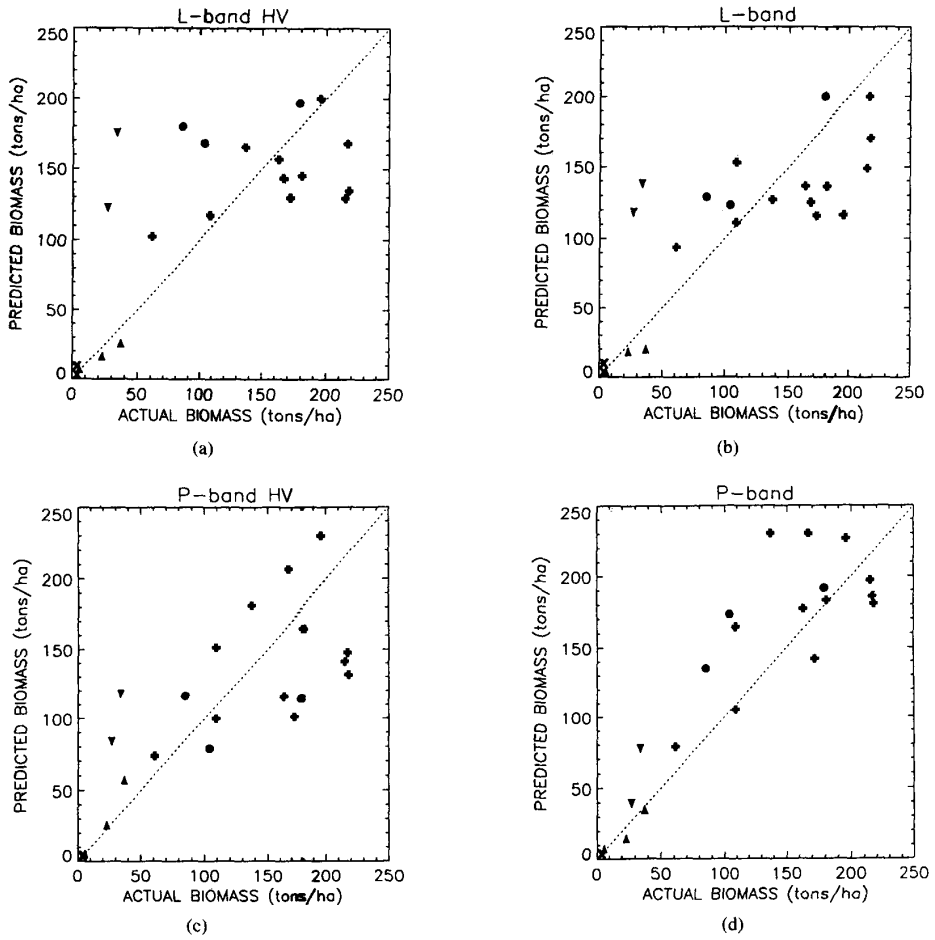

Fig. 4. Predicted biomass levels of various forest stands from BCEF versus actual biomass levels at (a) L-band HV-polarization; (b) L-band HH-, HV- , and VV-polarizations; (c) P-band HV-polarization; and (d) P-band HH- , HV- , and VV-polarizations.

TABLE II
ERRORS IN PREDICTED STANT BIOMASS ESTIMATES FROM THE RADAR AT VARIOUS FREQUENCIES AND POLARIZATIONS, AND ON DIFFERENT DATES. ERROR RATES ARE EXPRESSED IN PERCENTAGE OF ACTUAL STAND BIOMASS, EXCLUDING ALDER STANDS (BP6 AND AL1)

Frequency - Polarization(s)	Error on May 6, 1991	Error on July 21, 1993
P-band HV	29	32
P-band HH, HV, VV	21	19
L-band HV	39	27
L-band HH, HV, VV	35	20

analysis because WS41 and WS40 were not imaged in 1993 due to a reduction in swath width of the radar; and AL1 and BP6 suffered serious damage in 1992, leaving all alder trees permanently broken or laying flat on the ground. Hence, the summer estimates do not include alder stands (Table II). Nevertheless, the results are comparable to those obtained for the spring data, perhaps even slightly better in the summer. The major difference is that the inversion curves are different between the two dates (Section V).

For comparison, we performed a similar regression on the radar data collected over the Landes forest plantation, France [1]. The Landes forest plantation is more appropriate for biomass retrieval because trees are mono-species, very uniform in density, height, DBH, and age within each stand due to seeding and management practices. Stand biomass is known with 12.5% accuracy and is less than 150 tons/ha. The results show little data spread and an excellent retrieval of forest biomass from the radar (Fig. 5). The error rate is 11% at P-band whether one or three polarizations are used, 13% at L-band HV, and 20% at L-band using all three polarizations. In those areas of moderate biomass, σ°_{HH} and σ°_{VV} do not help improve the estimates obtained using only σ°_{HV}. It was understood that in natural forest ecosystems the accuracy of the inversion will be less because tree density, height, diameter and age as well as canopy structure have large spatial variations. At BCEF, standard deviation in biomass within each stand is 34% of the average stand biomass (Table I) and as high as 79% for BP14. Tree height, density, and height commonly vary by more than one order of magnitude from one plot to the next or even within the same plot. Hence, uncertainities in stand biomass increase with biomass and are very large for mature, tall forests. Actual uncertainties may even be larger considering that we ignore uncertainties associated with the use of empirical, allometric equations for computing tree biomass. Another complicating factor is that radar signals interact with more complex tree canopies of varying three-dimensional structure because the forest stands are not spatially homogeneous,

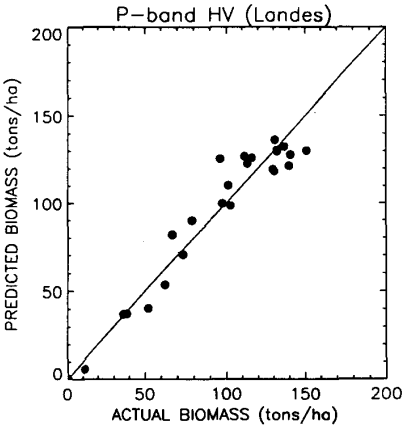

Fig. 5. Predicted biomass versus actual biomass for the Landes Forest, France [1], at P-band HV-polarization.

include tree gaps, old river sloughs, and a mixture of different tree species of various ages.

V. Temporal Dynamics

The radar backscatter from the forest is dependent on the seasonal and environmental conditions. As an illustration, Fig. 6 shows σ° from the forest on March 17, 1988 when the forest was frozen, and on July 21, 1993 when the forest was thawed and dry, with fully developed canopies. C-band data are not shown because they are less relevant to the retrieval of total aboveground biomass. A complete discussion of the radar scattering characteristics of the forest in the summer will be reported in a future paper. P-band data from March 17, 1988 are also not shown because they could not be absolutely calibrated with confidence. Fig. 6(a) shows that σ° at L-band may change by as much as 6 dB between spring and winter/frozen, which is as much as the sensitivity of σ°_{HV} to stand biomass. An inversion curve derived from winter/frozen data could not yield reliable estimates of biomass in spring. Similarly, σ° from the forest changes by several dB between spring [Fig. 2(b)] and summer [Fig. 6(b)], depending on the polarization, and regression curves for biomass retrieval again differ significantly between the two dates. At P-band, σ° from the forest in the summer [Fig. 6(c)] is several decibels lower than in spring [Fig. 2(c)].

Radar mapping of aboveground biomass is therefore dependent on seasonal and environmental conditions. At the same time, the temporal variability of σ° provides additional information about the forest. For instance between March 13 and March 17, 1988, the measured 6 dB change in σ° of the forest was due to a dramatic change in the dielectric constant of the tree trunks associated with the freezing of the fresh liquid water content of the trees on March 17 [18]. Hence, on March 17, the radar signals were sensitive to the frozen biomass, while on March 13, 1988 the radar signals were sensitive to the moist biomass of the forest. In the summer, the radar returns from the forest are lower presumably because the forest canopy and ground layers were drier than in early spring, and the radar signals were more attenuated during propagation through the canopy due to the presence of leaves on deciduous trees.

VI. Influence of the Incidence Angle

Another factor influencing the retrieval of forest biomass from the radar is the incidence angle of the radar illumination onto the forest. On May 6, 1991, AIRSAR imaged BCEF successively at

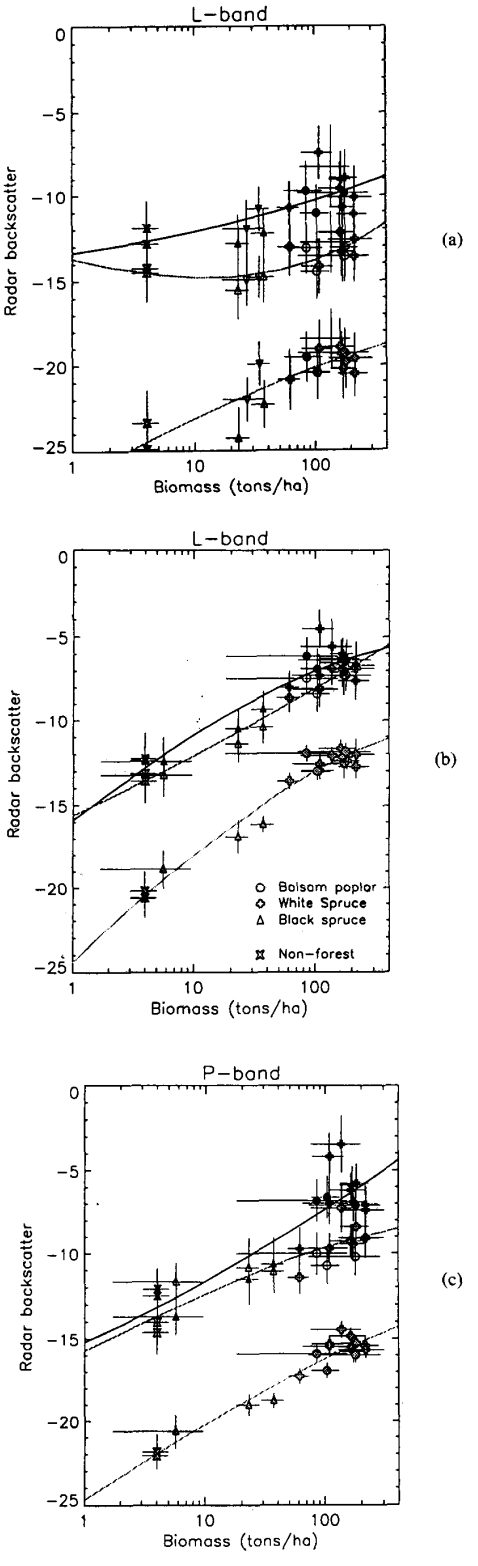

Fig. 6. σ° values of various forest stands versus whole-tree aboveground dry biomass (tons/ha) for SAR data acquired on (a) March 17, 1988 at L-band; (b) July 21, 1993 at L-band; and (c) July 21, 1993 at P-band.

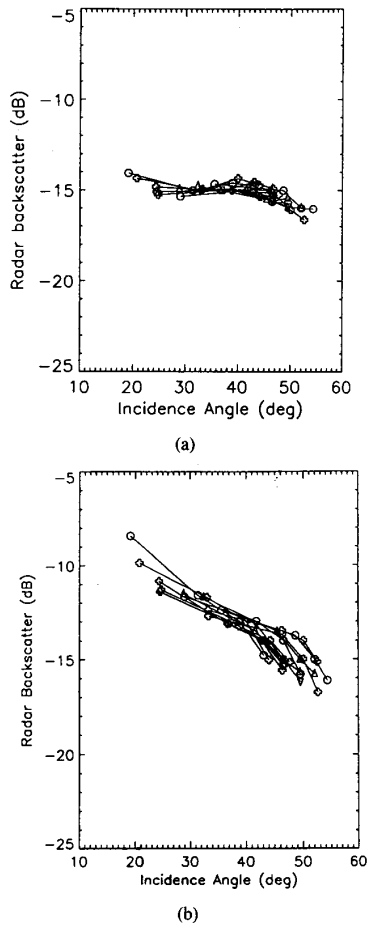

Fig. 7. σ° values of various forest stands versus the incidence angle of the radar illumination for multiple incidence angle SAR data acquired on May 6, 1991 at L-band (a) HV-polarization; and (b) HH-polarization. Continuous lines connect data points obtained from the same forest stand imaged at different look angles. A constant offset factor was applied on each line (a different constant factor for each stands) to facilitate interstand and comparison of the dependence of σ° on the incidence angle, regardless of the absolute level in radar backscatter of each stand. Symbols for various forest stands are the same as in Fig. 2.

four different look angles: $\theta = 23°$, 30°, 40°, and 50°. L-band data were calibrated using the radar response from two 1.8 m trihedral reflectors deployed in clear-cut areas prior to overflight. Data calibration could not be performed as accurately at P-band at the smaller look angles because the size and orientation of the corner reflectors were no longer optimal at that frequency and look angle; therefore only the L-band results are discussed here. Fig. 7 shows that between 25° and 50°, σ°_{HV} varies by less than 1 dB compared to 3–4 dB for σ°_{HH}. A smaller dependence of σ°_{HV} with the incidence angle θ_i is expected since the radar returns are dominated by volume scattering from tree branches which is less dependent on the incidence angle. At HH-polarization, σ° is more dependent on θ_i, probably because scattering from the tree trunks is more strongly varying with θ_i [4]. When $\theta_i < 25°$ or $\theta_i > 50°$, however, σ°_{HV} differs significantly from its average level at 30–50°. At those high and low angles, the radar will respectively underestimate and overestimate biomass if the effect of θ_i is ignored in the inversion. For instance, we examined the predicted biomass from three south-facing upland stands which were facing away from the radar on the May 6, 1991 flight, and for which $\theta_i = 53°$, 61°, and 58°. These stands, labeled PBW40 (Table I), BS21 (not listed), and PB41 (not listed) have a stand biomass of 103, 24, and 92 tons/ha, but the radar estimates are, respectively, 42, 4, and 16 tons/ha, i.e., significantly lower than the actual values. Hence, when $\theta_i > 50°$ or $\theta_i < 25°$, θ_i must be included in the inversion. A direct consequence is that topographic information will in general be required for reliable mapping of aboveground biomass over large areas.

VII. Conclusions

This study suggest SARs operating at long radar wavelengths have potential for mapping aboveground biomass of boreal forests in interior Alaska, a variable of prime importance to carbon cycling investigations, ecosystem studies and forest management applications. The error in predicted biomass from the radar is about 20% of the actual biomass at P-band. L-band signals do not perform as well because of more pronounced dependence on tree species (for instance alder trees), but the difference in performance between the two frequencies remains small. Prediction of forest biomass from the radar in monospecie forest plantations is 10% better, but this was an expected result. Data dispersion is more significant for natural forest ecosystems than for forest plantations because uncertainties in estimating aboveground biomass are larger in natural forests due to spatial variations in tree species, age, density, height, and DBH, and also because the radar signals interact with a canopy of spatially varying three-dimensional structure. Several other factors are also of importance for developing operational applications. One is that changing environmental conditions have a pronounced effect on radar backscatter from the forest, especially at the high northern latitudes where drastic changes occur. Hence, inversion curves derived at one geographical locations under different environmental conditions may be different. Secondly, digital elevation models should be combined with the radar data to improve radar estimates of forest biomass in areas of moderate topography.

Acknowledgment

The authors would like to thank Dr. T. LeToan, Universite Paul Sabatier, Toulouse, France, for her many comments on the manuscript and for sharing her ground truth data from the Landes site; Dr. J. Yarie, University of Alaska, Fairbanks, Dr. J. van Zyl, JPL, and several anonymous reviewers for reviewing the paper. We also thank the people from the AIRSAR group at JPL for collecting and processing of the data analyzed in this manuscript; V. Taylor and R. Carande for reprocessing of the P-band data; the Challenge Award Students T. Dilley, R. Weeded, J. Surmick, B. Olson, A. Meyer and V. Hoffman for participating in ground truthing of forest stands; Prof. Keith Van Cleve for sharing his biomass measurements for the LTER sites; B. Jaeger and J. Roth for leading the ground truth data collection in 1988 and 1990.

References

[1] T. Le Toan, A. Beaudoin, J. Riom, and D. Guyon, "Relating forest biomass to SAR data," *IEEE Trans. Geosci. Remote Sens.*, vol. 30, pp. 403–411, 1992.

[2] M. C. Dobson, F. T. Ulaby, T. Le Toan, A. Beaudoin, E. S. Kasischke, and N. Christensen, "Dependence of radar backscatter on conifer forest biomass," *IEEE Trans. Geosci. Remote Sens.*, vol. 30, pp. 412–415, 1992.

[3] E. S. Kasischke, L. L. Bourgeau-Chavez, N. L. Christensen, and M. C. Dobson, "The relationship between aboveground biomass and radar backscatter as observed on airborne SAR imagery," in *Proc. Third*

AIRSAR Workshop, Pasadena, CA, May 23-24, 1991, (JPL Pub. 91-30) pp. 11-21, 1991.
[4] J. J. van Zyl, "The effect of topography on radar scattering from vegetated areas," *IEEE Trans. Geosci. Remote Sens.*, vol. 31, pp. 153-160, 1993.
[5] A. Beaudoin, T. Le Toan, S. Goze, E. Nezry, A. Lopes, E. Mougin, C. C. Hsu, H. C. Han, J. A. Kong, and R. T. Shin, "Retrieval of forest biomass from SAR data," *Int. J. Rem. Sens.*, Sept. 1994.
[6] C. C. Hsu, H. C. Han, R. T. Shin, J. A. Kong, A. Beaudoin, and T. Le Toan, "Radiative transfer theory for polarimetric remote sensing of pine forest," *Int. J. Rem. Sens.*, Sept. 1994.
[7] K. McDonald, M. C. Dobson, and F. T. Ulaby, "Using MIMICS to model multiangle and multitemporal backscatter from a walnut orchard," *IEEE Trans. Geosci. Remote Sens.*, vol. 28, pp. 477-491, 1990.
[8] R. D'Arrigo, G. C. Jacoby, and I. Y. Fung, "Boreal forests and atmosphere-biosphere exchange of carbon dioxide," *Nature*, vol. 329, pp. 321-323, 1987.
[9] G. Bonan, "Atmosphere-biosphere exchange of carbon dioxide in boreal forest," *J. Geophys. Res.*, vol. 96, pp. 7301-7312, 1991.
[10] F. G. Hall, P. J. Sellers, M. Apps, D. Baldocchi, J. Cihlar, B. Goodison, H. Margolis, and A. Nelson, "BOREAS: Boreal ecosystem-atmosphere study," *IEEE Geosci. Remote Sens. Soc. Newslett.*, vol. 86, pp. 9-17, 1993.
[11] D. A. Lashof, "The dynamic greenhouse: feedback processes that may influence future concentrations of atmospheric trace gases and climatic change," *Climatic Change*, vol. 14, pp. 213-242, 1989.
[12] E. Sundquist, "The global carbon dioxide budget," *Science*, vol. 259, pp. 934-941, 1993.
[13] L. A. Viereck and K. Van Cleve, "Some aspects of vegetation and temperature relationships in the Alaska taiga," in *Proc. Conf.*, Fairbanks, AK, April 7, 8, 1982, School of Agriculture and Land Resources Management, Univ. Alaska, Fairbanks, Misc. Pub. 83-1, 1983.
[14] K. Van Cleve, L. Oliver, R. Schlentner, L. A. Viereck, and C. T. Dyrness, "Productivity and nutrient cycling in taiga forest ecosystems," *Can. J. For. Res.*, vol. 13, pp. 747-766, 1983.
[15] L. A. Viereck, K. Van Cleve, and C. T. Dyrness, "Forest ecosystem distribution in the taiga environment," in *Ecological Series Vol. 57, Forest Ecosystems in the Alaskan Taiga*, K. Van Cleve *et al.* Eds. New York: Springer-Verlag, 1986, pp. 22-43.
[16] C. W. Slaughter and L. A. Viereck, "Climatic characteristics of the taiga in interior Alaska," in *Ecological Series Vol. 57, Forest Ecosystems in the Alaskan Taiga*, K. Van Cleve, Ed. New York: Springer-Verlag, NY, 1986, pp. 2-21.
[17] J. J. van Zyl, R. Carande, Y. Lou, T. Miller, and K. Wheeler, "The NASA/JPL three-frequency polarimetric AIRSAR system," in *Proc. Int. Geosci. Remote Sens. Symp.*, Houston, TX, May 26-29, 1992, IEEE New York Pub., 1992. pp. 649-651.
[18] J. B. Way *et al.*, "The effect of changing environmental conditions on microwave signatures of forest ecosystems: Preliminary results of the March 1988 Alaskan aircraft SAR experiment," *Int. J. Remote Sensing*, vol. 11, pp. 1119-1144, 1990.
[19] J. J. van Zyl, "Calibration of polarimetric radar images using only image parameters and trihedral corner reflector responses," *IEEE Trans. Geosci. Remote Sens.*, vol. 28, pp. 337-348, 1990.
[20] D. L. Evans, J. J. van Zyl, and C. F. Burnette, "Incorporation of polarimetric radar images into multisensor data sets," *IEEE Trans. Geosci. Remote Sens.*, vol. 28, pp. 932-939, 1990.
[21] G. H. Manning, M. R. G. Massie, and J. Rudd, "Metric single-tree weight table for the Yukon territory," Information Rept. BX-X-250. Canadian Forestry Service, Pacific Forest Research Centre, Victoria, B.C., 60 pp., 1984.
[22] T. Singh, "Weight tables for important tree species in the Northwest territories," Forest management note N. 27, Canadian Forestry Service, Northern Forest Research Centre, Edmonton, Alto., 4 pp., plus tables, 1983.
[23] J. Yarie and K. Van Cleve, "Biomass and productivity of white spruce stands in interior Alaska," *Can. J. For. Res.*, vol. 13, pp. 767-772, 1983.
[24] E. Rignot and R. Kwok, "Characterization of spatial statistics of distributed targets in SAR data," *Int. J. Remote Sens.*, vol. 14, pp. 345-363, 1993.
[25] E. Rignot, C. William, J. B. Way, and L. Viereck, "Mapping of forest types in Alaskan Boreal forests using SAR imagery," *IEEE Trans. Geosci. Remote Sens.*, v. 32, pp. 1052-1060, this issue.

Retrieval Algorithms for Stratospheric Aerosols Based on ADEOS/ILAS Measurements

Sonoyo Mukai, Itaru Sano, Yasuhiro Sasano, Makoto Suzuki and Tatsuya Yokota

***Abstract*—This communication describes a procedure to estimate the vertical profiles of stratospheric aerosols based on the visible data to be obtained by ADEOS/ILAS. Our algorithms mainly consist of two parts: the first process is baseline estimation for the observed transmittance spectrum, followed by the inversion process that derives vertical profiles of atmospheric extinction from ILAS transmittance data.**

Model calculations with an ILAS simulator show that our treatment provides quick and accurate results within the expected domain of validity.

I. Introduction

This communication describes algorithms to estimate vertical distribution of stratospheric aerosol extinction based on the solar occultation measurements of the improved limb atmospheric spectrometer (ILAS), which will be installed on the advanced earth observing satellite (ADEOS) in 1996. It is well known that stratospheric aerosols play a dominant role in global climatic change [1]. Stratospheric aerosols are also important to the formation of high latitude clouds, such as the polar stratospheric clouds, and as tracers to study the dynamics of the stratosphere. For this reason, global-scale measurements of stratospheric aerosols are desirable [2]–[4].

ILAS is designed to measure vertical profiles of polar stratospheric trace gas, temperature, pressure, and aerosols by using two observing channels at the visible and infrared wavelengths covering $0.753 \sim 0.784$ μm and $6.2 \sim 11.8$ μm, respectively.

An inversion algorithm is a key process for our aerosol retrieval method [5]. The vertical structure inversion provides profiles of local atmospheric extinction from ILAS transmittance data. This is followed by a species separation step that decomposes the obtained total extinction into each component of the atmospheric constituents, i.e., air molecules and aerosols. It is shown that the retrieved pressure profiles from ILAS oxygen A-band analysis are available to improve and simplify the aerosol retrieval [6].

II. Retrieval Algorithms

ILAS measures the mean transmittance T_λ of the atmosphere at wavelength λ and tangent height h.

$$T_\lambda(h) = \exp\left[-\tau_\lambda(h)\right] = \exp\left[-\int_0^{l_0} \sigma_\lambda(l)\, dl\right], \tag{1}$$

$$\sigma_\lambda = \sigma_\lambda^{\mathrm{Ray}} + \sigma_\lambda^{\mathrm{O_2}} + \sigma_\lambda^{\mathrm{aero}} \tag{2}$$

Manuscript received October 26, 1993; revised March 7, 1994. This work was supported in part by the Japan Private School Promotion Foundation and the Environmental Science Research Institute, Kiniki University.

S. Mukai and I. Sano are with Kiniki University, Osaka 577, Japan.
Y. Sasano, M. Suzuki, and T. Yokota are with the National Institute for Environment Studies, Tsukuba 305, Japan.

IEEE Log Number 9403650.